Desalination and Water Treatment
www.deswater.com

doi: 10.5004/dwt.2018.21828

102 (2018) 165–172
January

Immersion time effects on the corrosion and passivation characterization of Ni–Cr glassy alloys in artificial seawater

Khadijah M. Emran[a,*], Hanaa Al-Refai[b]

[a]*Chemistry Department, College of Science, Taibah University, Al-Madinah Al-Monawarah, Saudi Arabia, Tel. +966 504355039; email: kabdalsamad@taibahu.edu.sa*
[b]*Chemistry Department, College of Science, Taibah University, Yanbu, Saudi Arabia*

Received 31 July 2017; Accepted 19 December 2017

ABSTRACT

Effects of immersion time on the passivation behavior and the pitting corrosion resistance of $Ni_{70}Cr_{21}Si_{0.5}B_{0.5}P_8C_{\leq 0.1}Co_{\leq 1}Fe_{\leq 1}$ (VZ1) and $Ni_{72.65}Cr_{7.3}Si_{6.7}B_{2.15}C_{\leq 0.06}Fe_{8.2}Mo_3$ (VZ2) glassy alloys in artificial seawater at different pH values have been studied using electrochemical impedance spectroscopy, cyclic polarization, and electrochemical frequency modulation techniques. The corrosion rate of the VZ1 alloy at all studied pH values reaches a low level after about 14 d and, for the VZ2 alloy, after 2 d of immersion. The VZ1 alloy has a relatively lower value of passive current density and represents a smaller anodic hysteresis loop area compared with the VZ2 alloy. The effect of immersion time on corrosion potential, corrosion current density, pitting potential, and repassivation potential has been investigated and discussed.

Keywords: Metallic glasses; Nickel base alloy; Artificial seawater; Immersion time

1. Introduction

Bulk metallic glasses (BMGs), or glassy metals, are considered to be the materials of the future [1]. This is attributed to their chemically and structurally homogeneous nature providing a lack of local electrochemically active sites [2]. They have many superior properties, including good soft-magnetic properties and excellent mechanical properties of high specific strength and large elastic limits (~2%) [3]. A good corrosion resistance is considered as one of the advantageous factors for metallic glasses. It is thought that high corrosion resistance combined with easy formability in the supercooled liquid region leads to the outstanding application potentials in place of traditional crystalline metals [4]. Ni-based BMGs, though comparative newcomers to the BMG family, they are considered as one of the most important BMG systems [5]. Nickel-based alloys are important to modern industry because of their ability to withstand a wide variety of severe operating conditions involving corrosive environments such as marine environment [6]. In chloride containing environments where nickel-based glassy alloys are prone to pitting corrosion under immersion conditions. The relative effectiveness of chromium, molybdenum, tungsten, and niobium on pitting corrosion can be assessed qualitatively by pitting resistance equivalent number (PREN), which is represented by the empirical equation [7,8].

$$\text{PREN} = \%\text{Cr} + 1.5\,(\%\text{Mo} + \%\text{W} + \%\text{Nb}) \quad (1)$$

It is well known that chromium spontaneously forms a protective passive film and provide good resistance to marine corrosion [9].

The corrosive effect of seawater has gained increased attention during the last few decades. Thus, it became of interest to carry out a laboratory study to evaluate the

* Corresponding author.

effects of marine environment on the corrosion behavior of Ni-based glassy alloys. The primary goal of this study is to characterize the Ni-based glassy alloys corrosion resistance in artificial seawater after different immersion periods using electrochemical impedance spectroscopy (EIS), cyclic polarization (CP), and electrochemical frequency modulation (EFM) measurements. A comparison of two alloys results under identical conditions can yield additional information on the influence of Cr percentage in Ni-based glassy alloys (as alloying element) on the corrosion resistance. The data from these tests were given as important information and better understand about these two alloys in marine environment.

2. Experimental section

2.1. Materials

Two Ni-based BMG alloys with nominal compositions of $Ni_{70}Cr_{21}Si_{0.5}B_{0.5}P_8C_{\leq 0.1}Co_{\leq 1}Fe_{\leq 1}$ (VZ1) and $Ni_{72.65}Cr_{7.3}Si_{6.7}B_{2.15}C_{\leq 0.06}Fe_{8.2}Mo_3$ (VZ2) (wt%) are investigated. The ingots' alloys were supplied by Vacuumschmelze and these glassy alloys were produced by rapid solidification as ribbons of about 40–74.5 mm width and 25 μm thickness.

The electrochemical measurements were carried out in aerated artificial seawater. A solution of artificial seawater was prepared by dissolving analytical grade reagents and double distilled water according to the Lyman and Fleming recipe, Table 1. All chemicals were obtained from Aldrich Chemical Co (Jeddah-KSA).

2.2. Methods

For electrochemical testing, the specimens of BMG alloys were evaluated under the same condition with a working area of 100 mm^2 of the bright face. The other side was coated with epoxy resin. Before each measurement, the working electrode was degreased with acetone, rinsed several times with doubly distilled water, cleaned in an ultrasonic bath, and finally connected to a copper specimen holder and immersed in the test solution. The electrochemical measurements were performed in a typical three-compartment glass cells containing three electrodes, the working electrode, which is the alloy under study, a platinum wire counter electrode, and a saturated Ag/AgCl as a reference electrode. Electrochemical measurements were conducted by means of an Interface 1000 TM, Gamry Potentiostat/Galvanostat/ZRA analyzer. Echem Analyst 5.58 software was used for plotting, graphing, and fitting data.

Table 1
Chemical composition of artificial seawater[a]

Salt	g kg^{-1}
NaCl	23.476
KCl	0.664
$CaCl_2$	1.102
$MgCl_2$	4.981
Na_2SO_4	3.917
$NaHCO_3$	0.192
KBr	0.096
$SrCl_2$	0.025
NaF	0.003
H_3BO_3	0.027

[a]Salinity is 34.481‰, pH adjusted to 7.5, 8, 8.2, and 8.5 with NaOH or HCl.

The potential of the examined alloy was recorded as a function of time for 1 h until it became stable. For the EFM technique the baseline frequency (b.f.) was 0.1 Hz, and input frequencies of 2 and 5 Hz were used, with amplitudes of 10 mV over four cycles, and the corrosion process under investigation is passive. The EIS measurements were carried out with a sinusoidal voltage of 10 mV and 10 points per decade. The frequency range was from 800 kHz to 0.1 Hz. For CP curves, the potential was scanned from cathodic to anodic directions after an impedance run in the range from –800 to 1.200 mV with sweep rate of 1 mV s^{-1}.

3. Results and discussion

3.1. Electrochemical impedance spectroscopy measurements in artificial seawater

Impedance spectra were recorded for the VZ1 and VZ2 alloys after different immersion periods (2, 6, 14, and 30 d) for each pH at 27°C. Impedance plots at 7.5, 8, 8.2, and 8.5 pH values for the VZ1 alloy were presented (Figs. 1(a)–(d)). All the complex diagrams show capacitive behavior characterized by an unfinished semicircle, implying a high corrosion resistance of the VZ1 alloy. The diameter of the capacitive arc obtained in the low-frequency region, which is attributed to the passivation mechanism occurring at the film/solution interface increases with increasing exposure periods in the range 2–14 d. After 30 d exposure and at all pH values, the Nyquist plot presented a more depressed arc which is different from that observed at lower exposure times. Nyquist plots for the VZ2 alloy show similar features to that of VZ1 (Figs. 1(e)–(h)). The diameter of the arc at low-frequency represents the resistance of inner passive film (R_f), decrease with increasing exposure periods from 2 to 30 d for all pH values. Bode plots for the VZ1 and VZ2 alloys exhibited two time constants with a broad phase maximum shifts to lower frequencies, which is a characteristic property of the passive surface [10].

Best fit was given by the model of equivalent electrical circuit with circuit description code $R_s(Q_1[R_{ct}(Q_2R_f)])$ as shown in Fig. 1(a). The values of the simulated EIS parameters are given in Table 2.

The values of oxide film resistance R_f are significantly greater than those for the charge transfer resistance R_{ct}, by more than 1×10^3 times, which points out to the presence of a protective oxide film providing a high corrosion resistance of VZ1 and VZ2 alloys. Therefore, the influence of R_{ct} on the total impedance of the interface seems to be comparatively negligible and, accordingly, the EIS data become dominated by the passive film properties.

For all pH values, the values of R_f regularly increase during 2–14 d due to the presence of the passive film on the surface, providing a protective layer (chromium oxide and/or nickel oxide) that is characterized by a low electrical

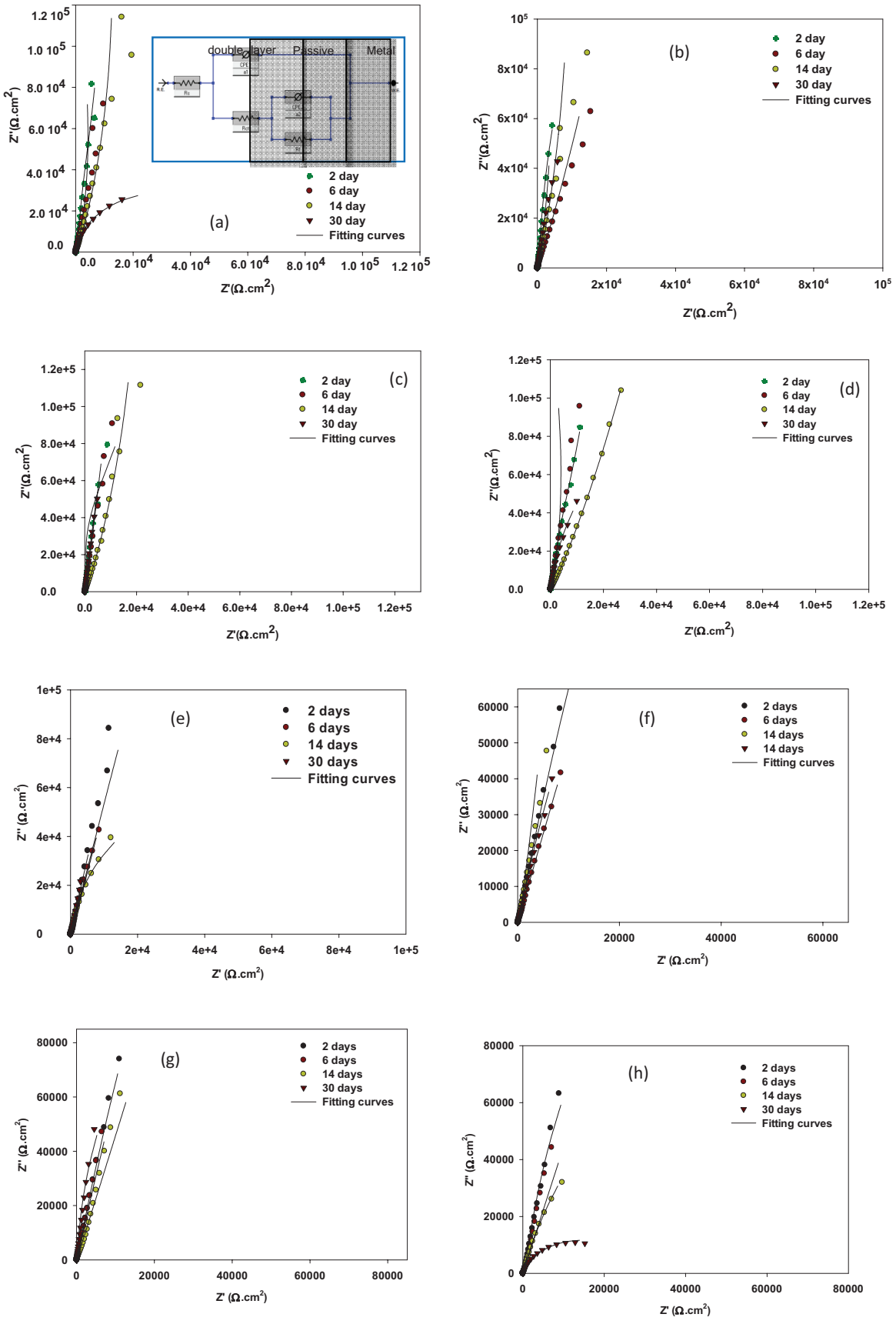

Fig. 1. Impedance spectra of VZ1 and VZ2 alloys for different immersion periods at 27°C.

Table 2
Equivalent circuit parameters for the spontaneously formed passive film on VZ1 and VZ2 alloy in artificial seawater at different pH values at 27°C

Alloy	pH	Period of immersion (d)	Charge transfer resistance (R_{ct}) (Ω cm^2)	Constant phase element CPE$_1$ ($\times10^{-5}$ Ω^{-1} cm^{-2}sn1)	n_1	Charge transfer resistance (R_f) (K Ω cm^2)	Constant phase element CPE$_2$ ($\times10^{-5}$ Ω^{-1} cm^{-2}sn1)	n_2
VZ1	7.5	2	30.34	1.483	0.873	2.644	1.248	0.873
		6	45.16	1.395	0.864	2.664	1.112	0.883
		14	4,233	1.041	0.838	7.615	1.003	0.678
		30	97.73	4.349	0.818	2.807	1.474	0.984
	8	2	94.65	2.511	0.822	2.130	9.541	0.924
		6	141.1	2.418	0.849	2.904	5.462	0.921
		14	820.1	1.399	0.809	5.877	1.239	0.820
		30	5.787	1.411	0.918	1.938	3.150	0.892
	8.2	2	6.764	2.921	0.871	1.828	9.127	0.838
		6	7.398	4.078	0.831	2.796	2.968	0.934
		14	7.908	1.344	0.880	4.256	1.954	0.852
		30	4.693	2.409	0.933	2.006	2.917	0.853
	8.5	2	209.1	2.673	0.821	2.593	7.055	0.946
		6	77.73	2.160	0.834	5.551	2.446	0.878
		14	1,294	2.036	0.812	6.602	1.051	0.919
		30	4.689	1.684	0.934	6.301	2.860	0.916
VZ2	7.5	2	54.76	2.007	0.791	3.274	1.486	0.950
		6	47.03	5.599	0.775	1.540	1.832	0.929
		14	54.89	3.625	0.843	1.202	1.882	0.846
		30	2.664	4.087	0.777	0.873	2.882	0.820
	8	2	8.157	1.346	0.883	5.336	1.880	0.854
		6	7.241	2.117	0.832	3.114	2.154	0.837
		14	6.796	2.930	0.871	0.824	4.961	0.838
		30	3.668	4.530	0.870	0.396	9.002	0.842
	8.2	2	20.89	1.340	0.880	2.881	1.958	0.852
		6	9.005	2.236	0.897	2.725	2.334	0.869
		14	6.451	3.692	0.827	2.224	2.841	0.808
		30	7.112	2.293	0.883	0.2986	2.982	0.809
	8.5	2	188.5	1.722	0.855	3.821	2.422	0.834
		6	134.4	5.022	0.858	3.678	4.496	0.812
		14	34.51	8.002	0.817	1.650	4.408	0.812
		30	18.46	8.913	0.844	0.417	4.874	0.874

conductivity and, thus, retards oxygen reduction (the main cathodic reaction). The passive film dissolution is initiated by Cl^- adsorption followed by alloying elements oxidation which releases a large amount of Ni^{2+} and/or Cr^{3+} nearby the surface, reaching supersaturation after a certain period (14 d), where the redeposition rate is higher than the dissolution rate, metal ions will tend to precipitate as hydrous oxide onto the surface providing a protective layer and an increase in dissolution resistance [11].

Over 30 d of exposure, the R_f decreases due to the *n*-type semiconductor inner barrier oxide layer formed on nickel-based alloys which is a good catalyst for oxygen reduction reactions. Reduction of R_f testifies rather to easier access of electrolyte to the VZ1 alloy (through the discontinuities of the layer of corrosion products). The CPE$_2$ values for VZ1 alloy decreases already mildly during 2–14 d and then increases in 30 d of exposure. This behavior may be related to the physical changes which take place inside the layer of corrosion products due to the reduction of the porosity of the layer of corrosion products formed on the surface of the VZ1 alloy or due to the growth of the passive film and increasing thickness of this layer. Long immersion periods (30 d) increase the exposure of VZ1 alloy surface to Cl^- ions, resulting in more available surface area of alloy lead to increase in film capacitance (CPE$_2$).

The inner film resistance R_f for VZ2 alloy decrease with increasing immersion times during 2–30 d. They reach lower values after a 30-d immersion for all pH values. This continuous decrease of corrosion resistance over time could be attributed to the slow production of Ni^{2+} and/or Cr^{3+} ions and their diffusion away from the surface, reducing the likelihood of corrosion product precipitation [11]. The long-term immersion can

preclude film growth process as the alloy undergoes passivity breakdown due to enhanced solubility of the corrosion products (interfacial film capacitance CPE_2 increasing), leading to a significant increase in surface film capacitance. The formation of Cr_2O_3 slows down the diffusion of oxygen and nickel in the oxide layer; the R_f value for VZ1 is higher than that for VZ2 alloy although the electrolyte used was similar.

To gain more information about the pitting corrosion resistance of the VZ1 and VZ2 alloys, CP curves at 7.5 pH value for a 2-d immersion period at 27°C are presented in Figs. 2(a) and (b). The curves recorded for other pH values were similar and have been omitted for better clarity of the figures. Analysis of the polarization data in Table 3 provides the following information about the VZ1 alloy: (1) corrosion current densities tend to decrease with increasing immersion time where the VZ1 alloy appear to have significantly lower corrosion current density during a period of about 14 d, then tend to increase after 30 d of exposure (Fig. 3(a)); (2) corrosion potentials are shifted in the more noble direction, with increasing immersion time; (3) the variations in the repassivation capacity range ($E_{pit} - E_{rep}$) and pit nucleation ($E_{pit} - E_{corr}$) of the VZ1 alloy with the change in immersion time usually do not follow a regular pattern; (4) a very small passive current density was observed where it varies from 0.1062 to 0.3453 mA cm^{-2} depending upon the immersion time; and (5) the lower i_{corr} value was determined at pH 8.5.

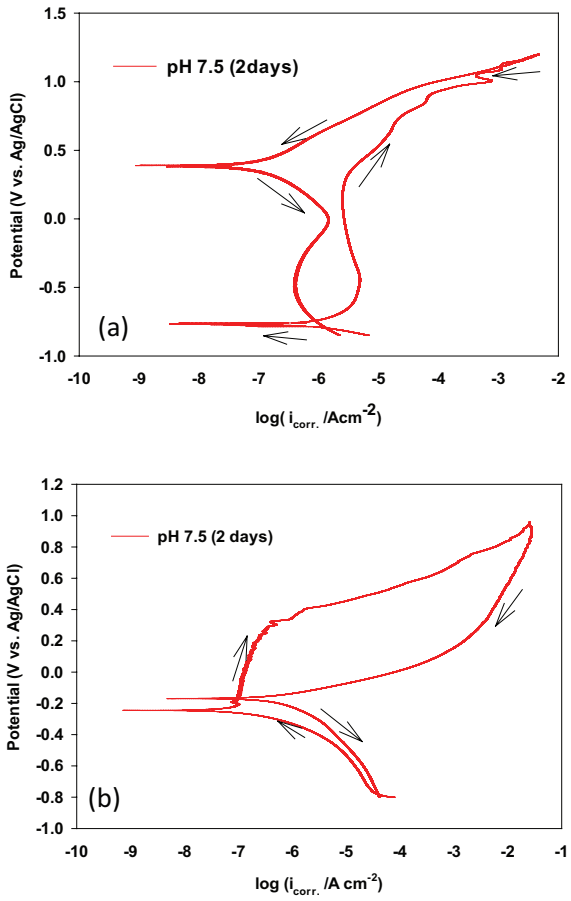

Fig. 2. Cyclic polarization curves of Ni-based glassy alloys at 7.5 pH for 2 d immersion period at 27°C.

The increase in the i_{corr} value after 30 d of exposure can be described as follows: increasing immersion time enhances the deposition of the corrosion products on the alloy (build-up on the surface) as a result of interaction between the artificial seawater and the alloy surface. These depositions act as a protective layer of a passive film. This can effectively seal the surface against further reaction (the most immediate common corrosion product is nickel hydroxide $Ni(OH)_2$) [12]. The partial cathodic reaction of the corrosion process is likely to be the reduction of hydrogen ion and water molecule according to the following equations (Eqs. (2) and (3)):

$$2H^+ + 2e^- \rightarrow H_2 \quad (2)$$

$$2H_2O + 2e^- \rightarrow H_2 + 2OH^- \quad (3)$$

Therefore, as the corrosion process continues, corrosion products continue to build-up and lead to an increase in the corrosion product thickness, which decreases the corrosion rate (decreases i_{corr}) at the 2–14 d. Long immersion periods increase the exposure of the VZ1 alloy surface to aggressive ions, such as the Cl^- ions, which exist in artificial seawater, resulting in reduced pitting corrosion resistance of the VZ1 alloy. In this condition, the corrosion product is not truly passivating as it acts as an oxide barrier layer membrane. The presence of Cl^- ions adsorbed on the weak parts of the corrosion product layer causes pitting which, subsequently, results in the initiation of pits and destroying the protective film on the alloy surface.

Analyzing the CP curves and the polarization data in Table 3 provides the following information about the VZ2 alloy: (1) for each pH, data for the corrosion current densities shows an almost clear trend where i_{corr} increased as an exposure times increased from 2 to 30 d (Fig. 3(b)); (2) no measureable trend of corrosion potential E_{corr} associated with pH over time was observed in the VZ2 alloy; and (3) the high repassivation capacity range, ($E_{pit} - E_{rep}$), revealed that the 7.3% Cr content of the alloy is not enough to provide pitting corrosion resistance in artificial seawater for different immersion periods. This explains the similar trend of EIS behavior observed for the VZ1 and VZ2 alloys.

The resistance for nickel-based alloys can be calculated from the alloying composition as the capacity of an alloy to resist pitting can be represented by the PREN according to Eq. (1) [7,8]:

PREN is represented by the relative effectiveness of chromium, molybdenum, tungsten, and niobium since these elements greatly improve their resistance to localized corrosion in seawater, where a higher potential is needed to initiate pitting in alloys with large PREN values than with alloys which have low values [13,14]. Nickel-based alloys with a PREN greater than 40 are very resistant to localized corrosion in natural seawater-immersed conditions. Our results support this argument. The results showed that the pitting corrosion resistance for the VZ1 alloy in seawater has a greater PREN (21) when compared with the value of 11.8 for the VZ2 alloy. The VZ1 alloy has a lower tendency to pitting or requires much higher potential to initiate pitting in the alloys. This behavior is the natural consequence of the dependence of pitting resistance on the PREN of the Ni-based glassy alloys

Table 3
Corrosion kinetic parameters for the VZ1 and VZ2 alloys at different immersion periods for each pH values in aqueous aerated artificial seawater at 27°C

Alloy	pH	Period of immersion (d)	EFM					CP				
			i_{corr} (mA cm^{-2})	$-\beta c$ (mV decade^{-1})	Corrosion rate × 10^{-3} (mmpy)	CF-2	CF-3	$-E_{corr}$ (mV)	i_{corr} (μA cm^{-2})	$-\beta c$ (mV decade^{-1})	E_{pit} (mV)	E_{rep} (mV)
VZ1	7.5	2	0.122	59	1.525	1.052	3.766	768.2	0.973	53	325.1	1,118
		6	0.121	53	1.506	1.853	3.545	415.5	0.027	56	55.83	1,089
		14	0.057	53	0.711	1.345	1.974	377.4	0.027	59	140.8	1,075
		30	0.395	56	4.934	3.776	2.284	334.5	0.271	56	419.9	1,063
	8	2	0.533	58	7.401	1.133	2.766	450.4	0.062	58	93.12	1,063
		6	0.462	55	5.017	1.327	1.365	431.1	0.041	58	371.4	1,098
		14	0.181	58	2.254	2.222	3.767	357.9	0.032	53	128.6	1,075
		30	0.684	59	8.529	2.926	2.447	269.1	0.091	54	225.7	1,045
	8.2	2	0.553	58	6.904	1.098	1.781	495.2	0.036	57	152.9	1,080
		6	0.419	52	5.231	1.950	1.153	367.9	0.031	51	134.7	1,055
		14	0.067	61	0.837	1.089	1.899	334.5	0.024	56	110.4	1,075
		30	0.087	58	1.094	2.180	2.243	385.8	0.051	57	166.9	1,083
	8.5	2	0.335	59	4.184	2.957	1.531	414.3	0.025	55	42.96	1,042
		6	0.166	53	2.074	2.980	1.987	454.8	0.024	58	328.9	1,080
		14	0.144	58	1.796	2.321	3.877	378.6	0.023	53	116.5	1,100
		30	0.293	59	1.170	3.784	3.887	448.5	0.050	55	286.7	1,069
VZ2	7.5	2	0.285	54	3.549	1.901	3.452	245.1	0.066	52	335	–160.2
		6	0.304	56	3.789	4.212	1.912	294.9	0.081	57	281.6	–162.9
		14	0.804	66	11.98	3.221	1.343	295.6	0.119	53	383.5	–191.7
		30	0.945	58	16.42	2.139	4.412	277.6	0.245	56	407.8	–150.5
	8	2	0.472	56	5.876	2.312	3.323	269.7	0.089	52	128.6	–120.1
		6	0.958	55	12.05	1.823	3.041	295.2	0.099	53	288.8	–162.2
		14	0.962	57	12.90	2.411	1.313	247.6	0.134	54	99.51	–191.7
		30	0.982	59	13.06	2.422	4.423	392.3	0.161	55	318.1	–111.7
	8.2	2	0.198	67	4.141	1.342	1.871	256.1	0.047	57	296.1	–184.5
		6	0.493	61	6.143	1.673	4.041	294.1	0.092	59	179.6	–184.5
		14	0.519	59	6.428	1.872	4.571	263.4	0.108	62	310.7	–92.23
		30	0.853	57	10.40	2.091	1.981	258.9	0.119	61	449.1	–38.82
	8.5	2	0.139	59	1.765	1.781	3.873	258.5	0.058	59	250.1	–186.9
		6	0.211	58	2.630	1.983	3.762	269.9	0.109	58	143.2	–206.3
		14	0.602	58	7.246	4.762	1.983	291.9	0.141	63	468.8	–132.3
		30	0.903	61	9.188	1.351	2.781	364.7	0.541	54	509.7	–106.8

indicating that the pitting corrosion resistance is greatly dependent on the composition of the alloys, particularly on Cr, Mo, and Ni contents.

To confirm the validation of the corrosion parameters measured by CP and EIS methods, the EFM technique was carried out. Table 3 shows the corrosion kinetic parameters obtained from the EFM measurements. The i_{corr} during 2–14 d decreased. Later, over 30 d of exposure i_{corr} increases. The results also show an outstanding corrosion resistance by having extremely low corrosion rates $0.7 \times 10^{-3} \leq$ (mmpy) $\leq 8.5 \times 10^{-3}$ even after exposures of about 30 d. These results indicate virtual immunity of the alloys toward artificial seawater environments. For the VZ2 alloy, the corrosion current density increase by increasing the immersion periods for each pH values and it exhibited an outstanding corrosion resistance as a result of the low corrosion rate (mmpy < 0.02). The deviation of causality factors from their ideal values might be due to the perturbation amplitude being too small, or that the resolution of the frequency spectrum is not high enough [15]. The results obtained from the EFM method are comparable and run parallel with those obtained from the EIS and CP methods.

3.2. Scanning electron microscope/energy dispersive X-ray spectroscopy analyses

The scanning electron microscope/energy dispersive X-ray spectroscopy (SEM/EDS) analyzed the surface morphology and confirmed the nominal composition of the VZ1 alloy in seawater of pH 7.5, 8, 8.2, and 8.5 after the CP

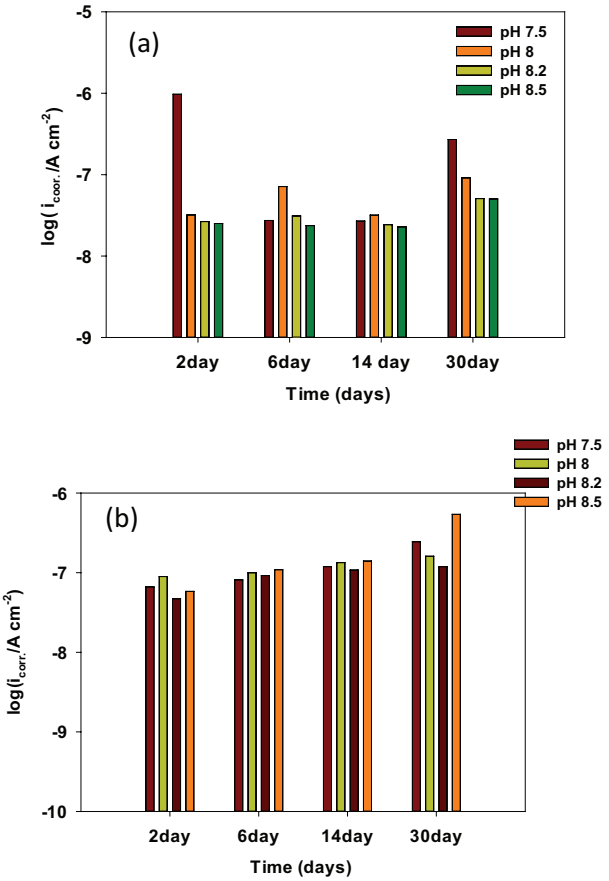

Fig. 3. Calculated values of i_{corr} during polarization at each immersion periods as a function of time (a) for VZ1 alloy and (b) for VZ2 alloy.

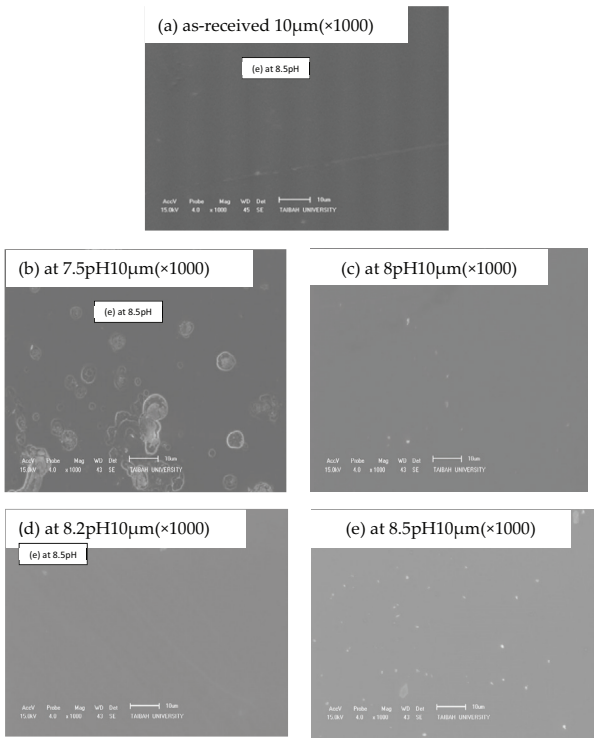

Fig. 4. Scanning electron microscope (SEM) morphology for the VZ1 alloy at various pH values in artificial seawater after 1 h at 27°C.

measurements (Fig. 4). The as-received surface of bulk glassy alloy (Fig. 4(a)) shows a smooth and uniform surface morphology, as the alloy was formed by cooling an alloy liquid with high cooling rates to avoid crystallization. Figs. 4(b)–(e) exhibit the passivating nature and high homogeneous oxide film, indicating high corrosion resistance. According to the EDS analysis (obtained curves are not shown), the precipitate was mainly composed of Ni, O, Cr, C, and P elements and they were uniformly distributed along the surface. The mass fractions of the chemical elements of the passive film (wt%) were as follows: Ni: 49.16, O: 19.57, Cr: 17.11, and C: 7.91; the atom ratio was about 2:4:1:3, of which the compositions can be expressed as $NiO + CrO_x$. These compositions were found in all the samples with EDS results which showed similar elemental mapping, proving that no other major corrosion product existed.

4. Conclusions

Two bulk glassy $Ni_{70}Cr_{21}Si_{0.5}B_{0.5}P_8C_{\leq 0.1}Co_{\leq 1}Fe_{\leq 1}$ (VZ1) and $Ni_{72.65}Cr_{7.3}Si_{6.7}B_{2.15}C_{\leq 0.06}Fe_{8.2}Mo_3$ (VZ2) alloys were tested in artificial seawater at different pH values. Both alloys appear to spontaneously passivate with a small active region, followed by a well-defined passive and transpassive regions at all pH values. The VZ1 alloy presented the lowest corrosion rate after 14 d of immersion at all pH values, whereas the corrosion rate of the VZ2 alloy shows a low level when immersed for 2 d. EIS analysis in artificial seawater media revealed that the influence of the charge transfer resistance, R_{ct}, on the total impedance of the interface seems to be comparatively negligible, and accordingly the EIS data become dominated by oxide film resistance, R_f. The VZ1 alloy is considered appropriate in industrial applications for its high pitting corrosion resistance of the VZ1 alloy in seawater and a wider range of passivation.

References

[1] D.C. Hofmann, L.M. Andersen, J. Kolodziejska, S.N. Roberts, J.P. Borgonia, W.L. Johnson, K.S. Vecchio, A. Kennett, Optimizing bulk metallic glasses for robust, highly wear-resistant gears, Adv. Eng. Mater., 19 (2017) 1600541–1600551.
[2] G. Liu, F. Wang, Y. Cao, Y. Sun, Potential prospective application of Zr-based bulk metallic glasses in dental implant, Mater. Trans., 56 (2015) 1925–1929.
[3] J.P. Chu, J.S.C. Jang, J.C. Huang, H.S. Chou, Y. Yang, J.C. Ye, Y.C. Wang, J.W. Lee, F.X. Liu, P.K. Liaw, Y.C. Chen, C.M. Lee, C.L. Li, C. Rullyani, Thin film metallic glasses: unique properties and potential applications, Thin Solid Films, 520 (2012) 5097–5122.
[4] D. Li, Z. Zhu, H. Zhang, A. Wang, Z. Hu, The influence of Zr substitution for Nb on the corrosion behaviors of the Ni-Nb-Zr bulk metallic glasses, Sci. China Phys., Mech. Astron., 55 (2012) 2362–2366.
[5] Y. Zeng, C. Qin, N. Nishiyama, A. Inoue, New nickel-based bulk metallic glasses with extremely high nickel content, J. Alloys Compd., 489 (2010) 80–83.
[6] H. Kim, D.B. Mitton, R.M. Latanision, Corrosion behavior of Ni-base alloys in aqueous HCl solution of pH 2 at high temperature and pressure, Corros. Sci., 52 (2010) 801–809.
[7] M.N. Rao, Pitting corrosion of sheets of a nickel-base superalloy, Mater. Corros., 60 (2009) 49–52.

[8] L.L. Machuca, S.I. Bailey, R. Gubner, Systematic study of the corrosion properties of selected high-resistance alloys in natural seawater, Corros. Sci., 64 (2010) 8–16.
[9] O. Lavigne, C. Alemany-Dumont, B. Normand, M.H. Berger, C. Duhamel, P. Delichére, The effect of nitrogen on the passivation mechanisms and electronic properties of chromium oxide layers, Corros. Sci., 53 (2011) 2087–2096.
[10] W.A. Badawy, K.M. Ismail, A.M. Fathi, Effect of Ni content on the corrosion behavior of Cu–Ni alloys in neutral chloride solutions, Electrochim. Acta, 50 (2005) 3603–3608.
[11] I.-W. Huang, B.L. Hurley, F. Yang, R.G. Buchheit, Dependence on temperature, pH, and Cl^- in the uniform corrosion of aluminum alloys 2024-T3, 6061-T6, and 7075-T6, Electrochim. Acta, 199 (2016) 242–253.
[12] F. El-TaibHeakal, A.M. Fekry, M.Z. Fatayerji, Influence of halides on the dissolution and passivation behavior of AZ91D magnesium alloy in aqueous solutions, Electrochim. Acta, 54 (2009) 1545–1557.
[13] J. Bhandari, F. Khan, R. Abbassi, V. Garaniya, R. Ojeda, Modelling of pitting corrosion in marine and offshore steel structures – a technical review, J. Loss Prev. Process Ind., 37 (2015) 39–62.
[14] A.U. Malik, N.A. Siddiqi, S. Ahmad, I.N. Andijani, The effect of dominant alloy additions on the corrosion behavior of some conventional and high alloy stainless steels in seawater, Corros. Sci., 37 (1995) 1521–1535.
[15] S.S. Abdel-Rehim, K.F. Khaled, N.S. Abd-Elshafi, Electrochemical frequency modulation as a new technique for monitoring corrosion inhibition of iron in acid media by new thiourea derivative, Electrochim. Acta, 51 (2006) 3269–3277.